https://doi.org/10.5194/egusphere-2025-3920
Preprint. Discussion started: 19 September 2025
© Author(s) 2025. CC BY 4.0 License.

Meltwater, mud, and the Mississippi: Upper Mississippi River Valley slackwater sediments reveal shifting deglacial meltwater sources associated with the Marquette Readvance of the Laurentide Ice Sheet

Shanti B. Penprase[1,2,3], Abigail C. Wilwerding[2], Andrew D. Wickert[2,3], Marion McKenzie[4], Phillip H. Larson[5,6], and Tammy M. Rittenour[7]

[1]Department of Earth Sciences, Dartmouth College, Hanover, NH 03755, USA
[2]Department of Earth & Environmental Sciences, University of Minnesota, Minneapolis, MN 55455, USA
[3]Saint Anthony Falls Laboratory, University of Minnesota, Minneapolis, MN 55414, USA
[4]Geology and Geological Engineering, Colorado School of Mines, Golden, CO 80401, USA
[5]Earth Science Programs, Department of Anthropology and Geography, Minnesota State University Mankato, Mankato, MN 56001, USA
[6]EARTH Systems Laboratory, Minnesota State University Mankato, Mankato, MN 56001, USA
[7]Department of Geosciences, Utah State University, Logan, UT 84322, USA

Correspondence: Shanti B. Penprase (shanti.b.penprase@dartmouth.edu)

Abstract. Meltwater from the Laurentide Ice Sheet changed course frequently over the last deglaciation, with impacts on local landscapes and global climate. However, a scale gap has confounded efforts to trace the sources and pathways of this meltwater: well-dated paleoceanographic records lack the precision of regional geological and geomorphic evidence, but local features are often dispersed and difficult to precisely date, making it challenging to construct a spatially distributed source-to-sink meltwater timeline. Here, we bisect this scale gap by using the upper Mississippi River network as a local integrator of upstream meltwater routing. We analyze a ∼400 cm core retrieved from a fluvial terrace near the mouth of the Whitewater River, a tributary to the Upper Mississippi River in southeastern Minnesota, where high water from meltwater floods deposited slackwater sediments. Optically stimulated luminescence (OSL) dates of 11.67±1.51 ka and 11.56±1.44 ka indicate that these slackwater sediments likely coincide with the Marquette Readvance of the Superior Lobe, a period when Laurentide Ice Sheet ice briefly reoccupied the Superior Basin, rerouting deglacial meltwater to the south. We geochemically fingerprint these sediments by applying Principal Component Analysis (PCA) and k-means clustering to X-Ray Fluorescence data, and find that Marquette-age meltwater flowed to the Mississippi first from the Glacial Lake Agassiz basin (rich in Ca) via the modern Minnesota River valley, and then from the Superior basin (rich in Fe, Cu, and Ni) via the glacial-stage St. Croix River. Weathering and post-depositional alteration obscure geochemical indicators of provenance in the top 200 cm of the core, which records the remainder of Marquette-age flood inundation. This study brings the pattern of ice-sheet retreat and associated meltwater routing into sharper focus and highlights the power of alluvial stratigraphy as an intermediary between local glacial geology and the marine sedimentary record.

https://doi.org/10.5194/egusphere-2025-3920
Preprint. Discussion started: 19 September 2025
© Author(s) 2025. CC BY 4.0 License.

1 Introduction

Terrestrial routing of Laurentide Ice Sheet-sourced glacial meltwater following the Last Glacial Maximum (LGM; ∼20 ka) remapped terrestrial hydrologic networks (Licciardi et al., 1999; Wickert, 2016), shaped landscape morphology (Knox, 1996; Faulkner et al., 2016; Penprase et al., 2025), and impacted global climate (Condron and Winsor, 2012; Ivanovic et al., 2018). These effects were felt strongly across the Mississippi River basin, which often received meltwater across an expanded drainage basin that extended, at times, from the Rocky Mountains in the west, to Hudson Bay in the north, and the Great Lakes to the east (Licciardi et al., 1999; Wickert, 2016). Records of this change, however, are often limited to local glacial records (e.g., Ridge, 1997; Breckenridge, 2013; Breckenridge et al., 2021) or continent-spanning data from marine sediment cores (Wickert et al., 2013, 2023; Williams et al., 2012). Here we seek to augment previous work by compiling data on an intermediate scale (e.g., Breckenridge and Johnson, 2009) that can link meltwater routing directions to their sources, thereby more closely tying ice-sheet and associated land-surface dynamics to freshwater delivery to the ocean.

Slackwater sediments are deposited at the mouths of tributaries due to inundation by water along the mainstem river. During the deglacial period, slackwater sediment deposition was triggered by pulses of glacial meltwater (Curry and Grimley, 2006; Johnson, 2009). Tributary inundation generates a lacustrine-like setting that allows glacially derived suspended sediments from the mainstem river to deposit in the tributary valley, including atop existing fluvial terraces. Slackwater sediments fortuitously preserve high-energy drainage events in a low-energy setting within a tributary connected to the main drainage (Curry and Grimley, 2006; Johnson, 2009). These preserved slackwater sediments thereby give stratigraphic context of provenance across regional sub-catchments and provide high-resolution, local records of the timing and provenance of glacial meltwater routing (Curry and Grimley, 2006; Johnson, 2009; Van Nest, 2014). As a result, slackwater records allow for comprehensive reconstructions of glacial meltwater routing and provide detail on the long-term evolution of landscape morphology and hydrologic changes triggered by deglaciation.

Local Quaternary geological mapping and geochronology constrain the timing of meltwater discharge from both Glacial Lake Duluth in the western Superior basin (Breckenridge, 2013) and Glacial Lake Agassiz (Fisher, 2003). These studies provide local geochronological constraints, but because of the rapid changes in meltwater routing during deglaciation, uncertainties in dating leave the relative chronology of meltwater routing unclear. At a greater scale, oxygen isotope records from the Gulf of Mexico tightly constrain the timing of meltwater discharge from the Mississippi River and may help to constrain the volumetric discharge itself (Wickert et al., 2013, 2023), while providing broad-scale provenance information (Sionneau et al., 2010). However, these continental scale data cannot easily provide detail about the detailed drainage evolution within a particular part of the Mississippi watershed. Slackwater deposits preserve stratigraphy, and therefore, a precise relative chronology of geochemically fingerprinted sediment supplied from different meltwater sources that also may be dated absolutely.

In this study, we examine a sediment core of slackwater sediments deposited atop a high terrace (20 m above the modern floodplain) near the mouth of the Whitewater River, an upper Mississippi River tributary. The core is comprised of four continuous core segments from 0 – ∼400 cm depth, with Core Segment 1 starting at 0 cm. We use optically stimulated luminescence (OSL) to date the sediments and collect X-Ray Fluorescence (XRF) data from the core segments, which we analyze using

https://doi.org/10.5194/egusphere-2025-3920
Preprint. Discussion started: 19 September 2025
© Author(s) 2025. CC BY 4.0 License.

Principal Component Analysis (PCA) and k-means clustering to determine changes in sediment geochemistry with depth and link changes in geochemistry to sediment provenance and deglacial meltwater spillway activation. Our goal is to answer two key questions:

1. Do the sediments in the sampled core preserve a geochemically distinct fingerprint that can be related to one or more upstream glacial meltwater sources and/or pathways?

2. How does geochemical variability in the core relate to localized shifts in glacial meltwater routing with ongoing ice-margin change during the deglacial period?

The results of this study provide a stratigraphic record of regional drainage reorganization and complement existing local glacial geological data and continental-scale meltwater-routing reconstructions. By leveraging the hierarchical network structure of rivers and their tributaries with a field site that is sensitive to two major meltwater pathways, we relate shifts in the ice margin directly to glacial meltwater streams through their downstream sedimentary records.

2 Background

2.1 Meltwater Routing Down the Upper Mississippi River Valley

Oxygen-isotope and terrestrial records show multiple kyr-scale periods of meltwater discharge down the Mississippi River during the most recent glacial and deglacial periods (Süfke et al., 2022; Wickert et al., 2023). Ice advance associated with the Last Glacial Maximum increased meltwater discharge down the Mississippi by 26 ka (Muller and Calkin, 1993; Clark et al., 2009; Wickert et al., 2023). As a result, ice-sheet-sourced sediment was long a major driver of aggradation along the Upper Mississippi River Valley, starting well before the Last Glacial Maximum and continuing until ∼18–16 ka, when sediment delivery paused (Knox, 1996; Carson, 2019). Continued periodic rise and fall in meltwater discharge to the Mississippi continued until 10.6 ka, when the ice margin retreated enough to route the previously Mississippi-bound meltwater eastward towards the Atlantic Ocean (Breckenridge and Johnson, 2009; Wickert et al., 2023; Karrow et al., 2000; Breckenridge, 2007).

As the Mississippi River aggraded, it raised base level for its tributaries, which aggraded in turn to meet it (Faulkner et al., 2016). Decades of field observations, supported by isotopic data, have noted numerous meltwater floods routed through the Mississippi River valley and generated during the retreat of the Laurentide Ice Sheet. These floods often originated from proglacial lake basins that breached a hydrologic barrier or constraint and resulted in initially sediment poor, high-magnitude discharge. Thus, these events drove significant incision into the landscape while simultaneously depositing slackwater sediments atop preexisting floodplains, fluvial terraces, and other landforms in tributary systems (Johnson, 2009; Van Nest, 2014; Fisher, 2003; Breckenridge, 2013).

During Laurentide Ice Sheet retreat, the Upper Mississippi River Valley received glacial meltwater inputs from two major sources: 1) a northeastern (NE) source via the Glacial St. Croix River, which received water from a number of glacial lobes and proglacial lakes, but most significantly from the Superior Lobe and lakes in the Superior Basin and 2) a northwestern (NW)

https://doi.org/10.5194/egusphere-2025-3920
Preprint. Discussion started: 19 September 2025
© Author(s) 2025. CC BY 4.0 License.

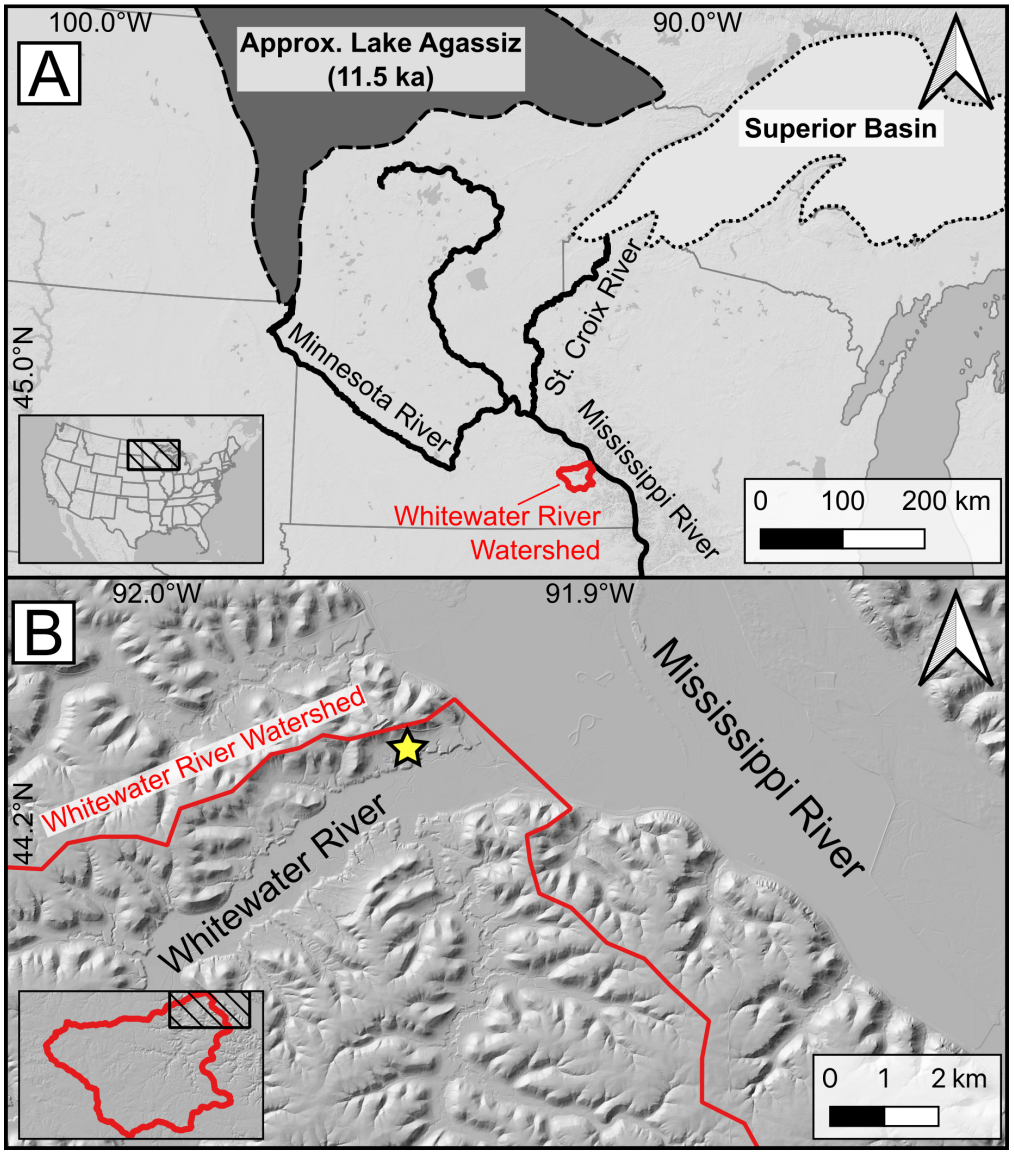

Figure 1. A) Approximate Glacial Lake Agassiz margin at 11.5 ka (dark gray; Dyke, 2004), the modern Superior Basin (light gray), the Minnesota River, the St. Croix River (including the Brule Spillway), the modern Mississippi River, and the Whitewater River watershed (red). B) The Whitewater and Mississippi River confluence with the core sampling location (yellow star).

https://doi.org/10.5194/egusphere-2025-3920
Preprint. Discussion started: 19 September 2025
© Author(s) 2025. CC BY 4.0 License.

source via Glacial River Warren (modern day Minnesota River; Upham, 1891), which received water from a series of proglacial lakes, including and most prominently, Glacial Lake Agassiz (Figure 1; Fisher, 2003; Blumentritt et al., 2009; Faulkner et al., 2016; Wickert, 2016; Gran et al., 2013; Fisher, 2020; Fisher and Breckenridge, 2022). While both sources experienced intervals of glacial meltwater delivery, due to differences in bedrock and catchment composition through which both glacial ice and meltwater was routed, each of these regions generated geochemically distinct sediments that can be identified in deposits (Curry and Grimley, 2006; Johnson, 2009; Wittkop et al., 2020). By examining the geochemistry, mineralogy, and stratigraphy of slackwater sediments in the Upper Mississippi River Valley, we can correlate these sediments to meltwater routing in the deglacial period. Although regional (e.g., Fisher, 2003; Blumentritt et al., 2009) and basin-wide studies (e.g., Wickert et al., 2023) indicate significant meltwater discharge from Glacial Lake Agassiz and Duluth to the Mississippi River, slackwater sediments have not been studied comprehensively this proximal to the most significant meltwater routing corridors of Glacial River Warren and the Glacial St. Croix River. Our dataset addresses a significant spatial gap and adds much needed chronologic and stratigraphic control to the meltwater routing events in the upper Mississippi River valley and how this landscape has evolved post-Last Glacial Maximum.

2.2 Slackwater sediments as an archive of meltwater floods

Within the Mississippi River valley and its tributaries, slackwater sediments have been the focus of several studies to further constrain glacial meltwater discharge chronology and connect these events to ice and sediment sources (Curry and Grimley, 2006; Van Nest, 2014; Johnson, 2009). Curry and Grimley (2006) identified slackwater sediments near St. Louis, MO, and tied the geochemistry and stratigraphy of these sediments directly to upstream shifts in glacial lobe margins. Within their slackwater cores, they identified Des Moines, Wadena, James, and Superior Lobe sediments, along with additional sediments from the Lake Michigan and Green Bay Lobes. These sediments were transported by meltwater from these source areas and were deposited ~800 km downstream of our study area (Figure 1). Curry and Grimley (2006) identified increased sedimentation from the Superior Lobe to the Mississippi River at 34 ka (29,600 ± 700 ^{14}C yr BP) and from the Wadena–Des Moines–James lobes at 25.5 ka (21,200 ± 80 ^{14}C yr BP; all radiocarbon dates are calibrated using Calib 8.20; Stuiver and Reimer, 1993 or IOSACal; Costa et al., 2022; both with the the IntCal20 curve; Reimer et al., 2020). Johnson (2009) examined slackwater sediments from the Mississippi River in northwestern Illinois (~300 km downstream from our study area) and additionally dated alluvial sediments below the slackwater deposits to 15.3 ka (12,840 ± 80 ^{14}C yr BP) and 15.6 ka (13,020 ± 45 ^{14}C yr BP). Within the slackwater sediments, Johnson (2009) identified Lake Agassiz-sourced sediments deposited closely after 15.5 ka that transition to fluvially reworked, glacially derived sediments from at least five pulses of meltwater with Superior-derived sediments at the top of the sequence. Van Nest (2014) studied sediment cores from Sny Bottom, a stretch of the Mississippi River in western Illinois ~600 km downstream of our study area, and identified a red-brown, silty clay cap of sediment associated with a Superior Basin source. Though direct radiocarbon dates were not available for these sediments, bracketing based on regional geochronology suggests that this final, Superior-origin pulse of glacial meltwater-induced slackwater deposition along the Mississippi River occurred sometime between 10.4–9.5 ka (Van Nest, 2014).

https://doi.org/10.5194/egusphere-2025-3920
Preprint. Discussion started: 19 September 2025
© Author(s) 2025. CC BY 4.0 License.

Table 1. Superior Basin sediments (NE) major geochemical fingerprints and associated citations.

Color	Red	Johnson (2009), Curry and Grimley (2006)
Source bedrock	Crystalline igneous	Wittkop et al. (2020), Curry and Grimley (2006)
Major elements	Fe, Cu, Ni	Thorleifson et al. (2007), Johnson (2009), Curry and Grimley (2006), Wittkop et al. (2020)
Additional elements	Y	Johnson (2009)
	Sr, Rb, Zr, Cr, Al, Na	Wittkopp et al. (2020)
	Zr, Cr, Co	Curry and Grimley (2006)
	Al, K, Mn, Rb, Sr, Ti, Zr	Thorleifson et al. (2007)
Major minerals	Kaolinite, chlorite	Johnson (2009)
	K-feldspar, magnetite	Curry and Grimley (2006)

2.3 Source-region geochemistry

2.3.1 Northeastern (NE) Source: Superior Basin via the Glacial St. Croix River

Northeastern, Superior Basin-derived sediments (Table 1), routed down the Glacial St. Croix River, were largely sourced from mafic igneous bedrock (Curry and Grimley, 2006; Thorleifson et al., 2007) enriched in ferromagnetic and heavy minerals (Thorleifson et al., 2007) with high magnetic susceptibility (Johnson, 2009). These sediments are typically red and contain high iron (Fe) (Lively and Thorleifson, 2009; Wittkop et al., 2020; Johnson, 2009; Curry and Grimley, 2006), copper (Cu) (Johnson, 2009; Lively and Thorleifson, 2009), and Nickel (Ni) (Lively and Thorleifson, 2009) concentrations, as shown by state geological mapping (Figure 2; Lively and Thorleifson, 2009). Preserved glacial tills in this region are enriched in aluminum (Al), iron (Fe), potassium (K), manganese (Mn), nickel (Ni), rubidium (Rb), strontium (Sr), titanium (Ti), and zirconium (Zr) relative to the Agassiz basin sediments (Thorleifson et al., 2007; Lively and Thorleifson, 2009). Superior-basin sediments also have higher yttrium (Y) (Johnson, 2009), Fe_2O_3 and Na_2O + K_2O and lower CaO relative to other, regional glacial sediment sources (Wittkop et al., 2020). Superior-derived sediments have high potassium feldspar and plagioclase feldspar content, in addition to high levels of kaolinite and chlorite (Curry and Grimley, 2006; Thorleifson et al., 2007; Johnson, 2009).

For the purposes of this study, we focus on the heavy metals Fe, Cu, and Ni as markers for Superior Basin sediments, based on available elements from XRF analysis and due to the consistent linkages between Fe, Cu, and Ni with the Superior Basin in previous studies (Lively and Thorleifson, 2009; Thorleifson et al., 2007; Wittkop et al., 2020; Curry and Grimley, 2006; Johnson, 2009).

2.3.2 Northwestern (NW) Source: Glacial Lake Agassiz via Glacial River Warren

Northwestern, Glacial Lake Agassiz-derived sediments (Table 2) flowed through Glacial River Warren (modern Minnesota River) into the Upper Mississippi River Valley. These glacial sediments are derived from regional bedrock that includes cre-

https://doi.org/10.5194/egusphere-2025-3920
Preprint. Discussion started: 19 September 2025
© Author(s) 2025. CC BY 4.0 License.

Table 2. Agassiz Basin sediments (NW) major geochemical fingerprints and associated citations.

Color	Gray	Johnson (2009), Curry and Grimley (2006)
Source bedrock	Carbonates, shales	Wittkop et al. (2020), Curry and Grimley (2006)
Major element	Ca	Thorleifson et al. (2007), Johnson (2009), Curry and Grimley (2006), Wittkop et al. (2020)
Additional elements	Se, Cd	Johnson (2009)
	Al, S, Mn, Ca, Mg, V, Cr, Mn, Ba, Zn, Pb	Wittkopp et al. (2020)
	Se	Curry and Grimley (2006)
Major minerals	Expandable clays	Johnson (2009)
	Clays, quartz, low magnetite	Curry and Grimley (2006)
	Barite, pyrite	Thorleifson et al. (2007)

taceous shale and carbonates (Curry and Grimley, 2006; Thorleifson et al., 2007; Wittkop et al., 2020). Sediments from the Agassiz region are typically fine-grained, clay-rich, and buff to gray (Thorleifson et al., 2007; Wittkop et al., 2020; Johnson, 2009). Agassiz basin sediments have greater abundance of calcite and dolomite than Superior-basin material (Thorleifson et al., 2007; Johnson, 2009; Wittkop et al., 2020), with 26.2–45.3% carbonate content in Agassiz basin sediments compared to 11.2–17.3% for Superior derived sediments (Johnson, 2009). In addition, Agassiz basin sediments include several key clay minerals, including illite and expandable clay species (Curry and Grimley, 2006; Johnson, 2009) and have relatively low abundances of feldspar minerals (Curry and Grimley, 2006). Elementally, Agassiz-derived sediments are rich in calcium (Ca) (Lively and Thorleifson, 2009; Johnson, 2009) as well as selenium (Se) (Curry and Grimley, 2006; Johnson, 2009) and cadmium (Cd) (Lively and Thorleifson, 2009; Johnson, 2009). The high concentrations of Ca found in sediments from the Agassiz region are reflected in geochemical maps, which show elevated Ca in the western portion of Minnesota (Figure 2; Lively and Thorleifson, 2009) and the region is underlain by carbonate bedrock (Lively and Thorleifson, 2009; Thorleifson et al., 2007; Wittkop et al., 2020; Curry and Grimley, 2006; Johnson, 2009). As a result, we use Ca as a marker for the NW, Agassiz region.

2.4 Field Setting: Whitewater River and the Upper Mississippi River

We collected core sediments from a terrace surface within the Whitewater River valley near the confluence with the Mississippi River. The sampling location is upstream of the Curry and Grimley (2006), Johnson (2009), and Van Nest (2014) study areas, thereby addressing a spatial gap in our data and understanding of meltwater routing through the Mississippi River valley. The Whitewater River Basin lies in the "Driftless-Like Topography" physiographic region in southeastern Minnesota and on the edge of the Driftless Area, which was never glaciated (Carson et al., 2019). The "Driftless-Like Topography" region was not glaciated at the LGM but does have sparse pre-Illinoian glacial till and erratics in the uplands (older than MIS 8, ca. 300 ka; Carson et al., 2019).

The Whitewater River catchment is underlain by Paleozoic sandstone, shale, dolostone, and limestone (Runkel, 1996). The terrace surface we sampled grades to the Savanna terrace level (Flock, 1983; Knox, 2007), based on published age of terraces

https://doi.org/10.5194/egusphere-2025-3920
Preprint. Discussion started: 19 September 2025
© Author(s) 2025. CC BY 4.0 License.

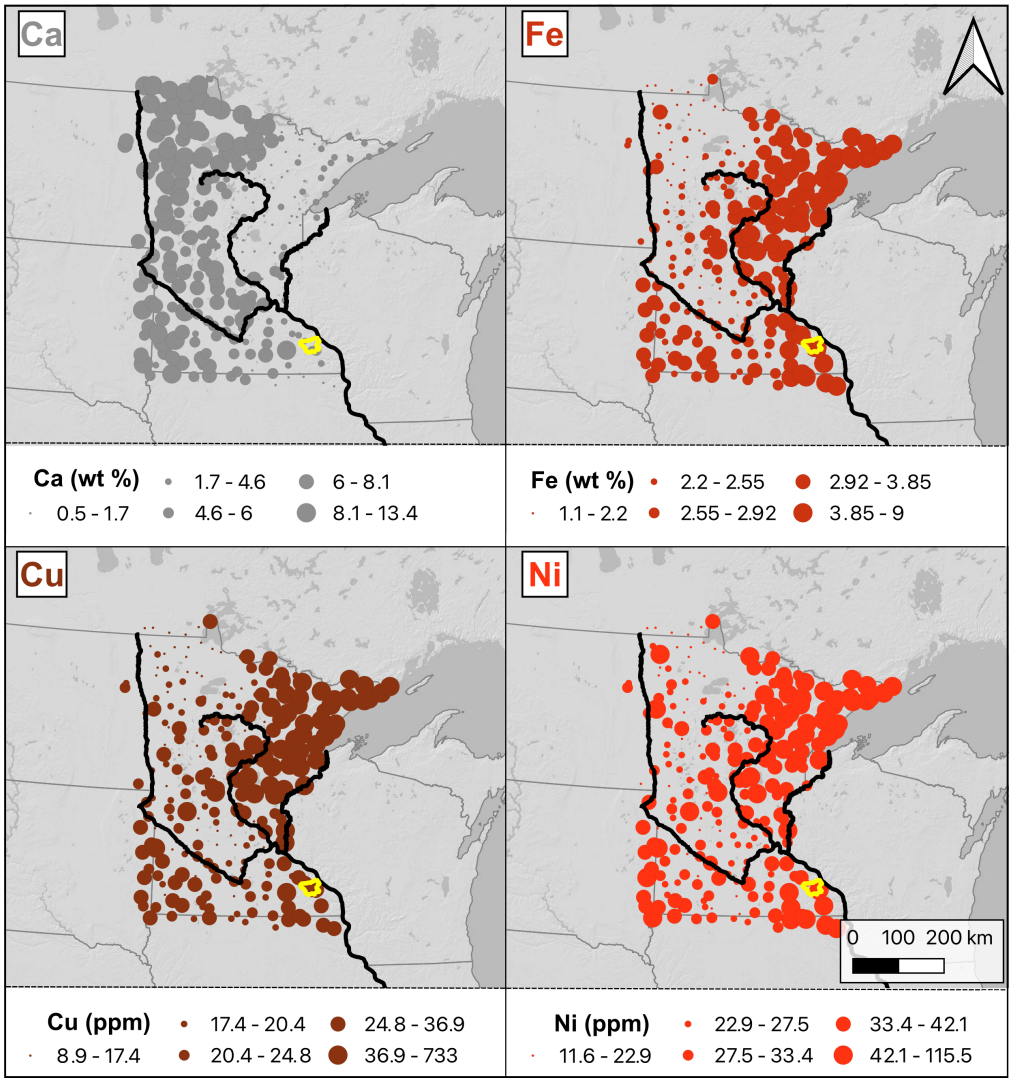

Figure 2. Soil parent material geochemistry, as measured in C-horizon till samples, for the state of Minnesota via the Minnesota Geological Survey (Lively and Thorleifson, 2009) for the elements of interest in this study, major rivers (black), and Whitewater River watershed (yellow). Elevated Ca is associated with the NW, Agassiz source while elevated Fe, Cu, and Ni are associated with the NE, Superior source. Marker size denotes quantity, with larger markers indicating higher quantities present in sample material. Units for each map are given in the key.

https://doi.org/10.5194/egusphere-2025-3920
Preprint. Discussion started: 19 September 2025
© Author(s) 2025. CC BY 4.0 License.

of the same elevation within the Whitewater catchment (Penprase et al., 2025). Previous studies sampling river terraces in the Whitewater River Valley have identified local alluvium as quartz-rich and sandy (Penprase et al., 2025), largely sourced from the Jordan Formation, a local quartz-rich, sandstone within the catchment (Runkel, 1996). The modern Whitewater River has a sandy riverbed dominated by sediment derived from this lithologic formation, resulting in elevated silica concentrations in locally-derived sediments. As a result, we use high Si values as a marker for local sediments in this study.

3 Methods

3.1 Field Sampling

We used a Geoprobe hydraulic push core rig to extract four continuous, 3.81 cm (1.5 in) diameter, 122 cm (4.0 ft) long sediment core segments in clear plastic liners to generate a continuous sediment record down to 412.6 cm depth. We completed the initial sediment description from remnant Geoprobe bit material in the field before packing and capping the core segments for additional laboratory analysis. We split the sediment core segments and completed detailed sediment descriptions at the University of Minnesota Surface Processes Laboratory. We determined texture by making a qualitative assessment of sediment composition using diagnostic descriptions based on the fraction of clay, silt, and sand. We then collected high-resolution core segment images at the Continental Scientific Drilling (CSD) Facility at the University of Minnesota using a Geotek Core Imaging System and calibrated color and grayscale patches (Figure 3).

To date the timing of sediment deposition, we collected two OSL samples, at ∼150 and ∼250 cm depth, using a hand auger and metal sampling bucket on the same terrace surface, approximately 300 cm away from the sediment core sampling location. Target depths were informed by initial Geoprobe sediment core descriptions. During hand auger sampling, we used these sediment descriptions to ensure stratigraphy between the OSL and the sediment cores were in agreement. At each target depth, we first collected a bucket of sediment for the dose rate sample, then used a closed metal auger bit containing an aluminum OSL tube to collect the equivalent dose sample, ensuring it was fully packed. The depth of the hole ensured no sunlight would prematurely bleach equivalent dose samples and filled sampling tubes tubes were shielded from sunlight and capped in the field. A second dose rate sample was collected below the equivalent dose depths and all dose rate samples were homogenized in the lab to create a single dose rate sample for each OSL sampling depth. In addition, the outermost material of the equivalent dose tube was excluded from equivalent dose analysis to avoid any risk of sediment exposure to sunlight.

At the time of OSL sampling, final XRF data were not yet available to identify geochemical provenance within the core stratigraphy. However, prior work (Penprase et al., 2025) dated the underlying terrace fill and surface abandonment age to provide bracketing age bounds between 13.8 ka and 10.6 ka. This age window agrees with regional chronologies for slackwater deposition down the upper Mississippi River Valley (e.g., Van Nest, 2014; Wickert et al., 2024; Lepper et al., 2013). Given this narrow window and the inherent error margins of OSL dating, high-resolution sampling at every stratigraphic contact would have been both inefficient and fiscally impractical, as results would overlap substantially. Thus, our sampling strategy prioritized obtaining reliable ages to constrain the overall period of slackwater deposition, rather than dating each stratigraphic unit. Detailed provenance variability within this interval is better resolved through higher-resolution methods such as XRF.

https://doi.org/10.5194/egusphere-2025-3920
Preprint. Discussion started: 19 September 2025
© Author(s) 2025. CC BY 4.0 License.

3.2 Optically Stimulated Luminescence (OSL)

We processed the two OSL samples (∼150 and ∼250 cm depth) at the Utah State University Luminescence Laboratory following standard laboratory protocols under amber-light conditions. Due to the high clay content, we treated each equivalent dose sample with HNO_3 to deflocculate and break up the sediment. Once deflocculated, we sieved each sample to isolate the 150–250 μm fraction and purified the sieved sediments to remove carbonates and organics using HCl and H_2O_2. To isolate quartz grains, we completed gravity separation using sodium polytungstate ($N_6O_{39}W_{12}$, 2.72 g cm^{-3}) before final etching in HF. We divided the etched quartz grains into aliquots (∼20 per disc) and mounted them on stainless steel discs for analysis. The samples were then analyzed using a Risø TL/OSL DA-20 reader with standard instrument settings and following the single-aliquot regenerative-dose procedure (Murray and Wintle, 2000). We selected water-content percentage based on collected water-content samples in combination with an interpreted moisture content over burial history for these sediments. Dose-rate samples were randomly split and analyzed using ICP-MS and ICP-AES techniques to determine U, Th, K, and Rb components (Table 3). Total dose rate values included attenuation from water content and cosmic dose contribution based on sample depth and geospatial location (Durcan et al., 2015). We calculated luminescence ages using the Central Age Model (Table 3; Galbraith and Roberts, 2012).

3.3 X-Ray Fluorescence (XRF), *k*-Means Clustering, and Principal Component Analysis (PCA)

To measure the depth-dependent elemental composition of the sediment core segments, we collected X-Ray Fluorescence (XRF) data and X-Radiographic Images at the Large Lakes Observatory, University of Minnesota Duluth, using an ITRAX XRF Core scanner. We scanned each core segment for XRF at 0.2 cm resolution with a 15 second dwell time while simultaneously capturing X-radiographic images to determine the relative concentration in counts of 32 elements. Data points received a 1 (valid) or 0 (invalid) data validity value during collection; invalid (0) data points and data points with no geochemistry values were excluded from analysis.

Based on the major elements present in each source area, in this study we focused on five elements of interest (Si, Ca, Fe, Cu, and Ni) which are strongly associated with Local (Si), Agassiz (Ca), or Superior (Fe, Cu, and Ni) source areas. To determine the elemental variability and find correlations within the XRF data, we performed two-dimensional principal component analysis (PCA) using R for the five elements of interest (Si, Ca, Fe, Cu, and Ni). PCA generates axes (PC1 and PC2) that identify the major drivers of variability in a dataset and plots the parameters of the data as vectors, with vectors of similar orientation correlating closely, orthogonal vectors uncorrelated, vectors plotting 180 degrees indicating an inverse correlation between factors, and the location of individual points in the plot indicating the relative concentration of each element for that specific depth in the core. To delineate grouping within the dataset and which data points are most closely associated with each other, we then applied k-means clustering to the PCA output, with an elbow test (Figure S2) to determine an appropriate number of groupings (k) for the dataset. k-means clustering delineates groups and classifies data points within a dataset by identifying groupings that minimize the distance between points and their associated cluster center. We associated resultant groupings with the three possible sediment provenances (Local, Agassiz, and Superior). With the data points in the dataset classified, we then

https://doi.org/10.5194/egusphere-2025-3920
Preprint. Discussion started: 19 September 2025
© Author(s) 2025. CC BY 4.0 License.

Table 3. Optically Stimulated Luminescence (OSL) Age & Dose Rate Information

Sample	Lab num.	Depth (m)	Num. of aliquots[2]	Over-dispersion (%)	Dose Rate (Gy/ka)	Equivalent Dose[3] ± 2σ (Gy)	Age ± 2σ (ka)
WW_2021101_Weaver_1	USU-3770	1.16–1.39, 1.44–1.64[1]	16 (19)	16±4	2.65±0.11	30.89±3.11	**11.67±1.51**
WW_2021101_Weaver_2	USU-3771	2.36–2.59	22 (38)	18±4	2.35±0.09	27.13±2.60	**11.56±1.44**

Sample	Lab num.	Depth (m)	H_2O[4] (%)	K[5] (%)	Rb[5] (ppm)	Th[5] (ppm)	U[5] (ppm)	Cosmic (Gy/kyr)
WW_2021101_Weaver_1	USU-3770	1.16–1.39, 1.44–1.64	25.0 (27.4)	1.87 ± 0.05	89.0 ± 3.6	11.0 ± 1.0	2.5 ± 0.2	0.18 ± 0.02
WW_2021101_Weaver_2	USU-3771	2.36–2.59	25.0 (31.0)	1.87 ± 0.05	73.4 ± 2.9	7.2 ± 0.6	1.8 ± 0.1	0.16 ± 0.02

[1] During sampling for the shallower OSL sample, the first equivalent dose sampling tube (1.16–1.39 m) was unexpectedly partially filled (∼50%). This sample was packed and labeled as the upper equivalent dose sample. As we had collected a lower dose rate sample at this time (1.39–1.44 m), we then collected a second equivalent dose sample (1.44–1.64 m). We examined the sediments at these depths in detail in previous auger and drilling holes as well as during OSL sampling and determined that the material in this section was homogeneous, allowing for this sampling procedure. Both equivalent dose samples were combined in the lab, creating a gap in the sampling depth

[2] Age analysis using the single-aliquot regenerative-dose procedure of Murray and Wintle (2000) using 1-mm aliquots of quartz sand (150–250 μm). Number of aliquots used in age calculation and number of aliquots analyzed in parentheses.

[3] Equivalent dose (DE) calculated using the Central Age Model (CAM) of Galbraith and Roberts (2012).

[4] In-situ values in parentheses, with the value reported outside the parentheses used as moisture content over burial history.

[5] Radioelemental concentrations determined using ICP-MS and ICP-AES techniques; dose rate is derived from concentrations using conversion factors from Guérin et al. (2011).

generated a plot of depth distribution by cluster to delineate depth-variable prevalence of each provenance grouping, allowing us to visualize changes in dominant sediment source with changes in depth.

4 Results

4.1 Optically Stimulated Luminescence (OSL) Results

OSL ages place the timing of deposition at ∼11.6 ka, with the shallower OSL sample (∼150 cm depth) providing an OSL age of 11.67 ± 1.51 ka and the deeper sample (∼250 cm depth) providing an age of 11.56 ± 1.44 ka (Figure 3, Table 3). Equivalent dose measurements in the OSL analysis show a cluster of values with no obvious outliers (Figure S1), indicating that the sediments were well bleached prior to deposition and that the central age model is appropriate for age calculations.

4.2 Core Sedimentology

Core sedimentology is distinctly different from fluvial terrace sediments collected in other regions of Whitewater River (Penprase et al., 2025) and is dominated by two major clay lithologies not found in other sediment core segments from the catchment: a red metallic-rich clay and a gray dolomitic clay. These two clay types transition into quartz-rich sand at the bottom of the core (examples indicated in Figure 3). X-Radiographic images show alternating densities, as indicated by high density (black) and low density (white) shading throughout the core segments (Figure 3). Starting at the base of the sediments (412.6 cm), the core contains sandy alluvium and bedding typical to other terrace surfaces within the Whitewater catchment (Figure

https://doi.org/10.5194/egusphere-2025-3920
Preprint. Discussion started: 19 September 2025
© Author(s) 2025. CC BY 4.0 License.

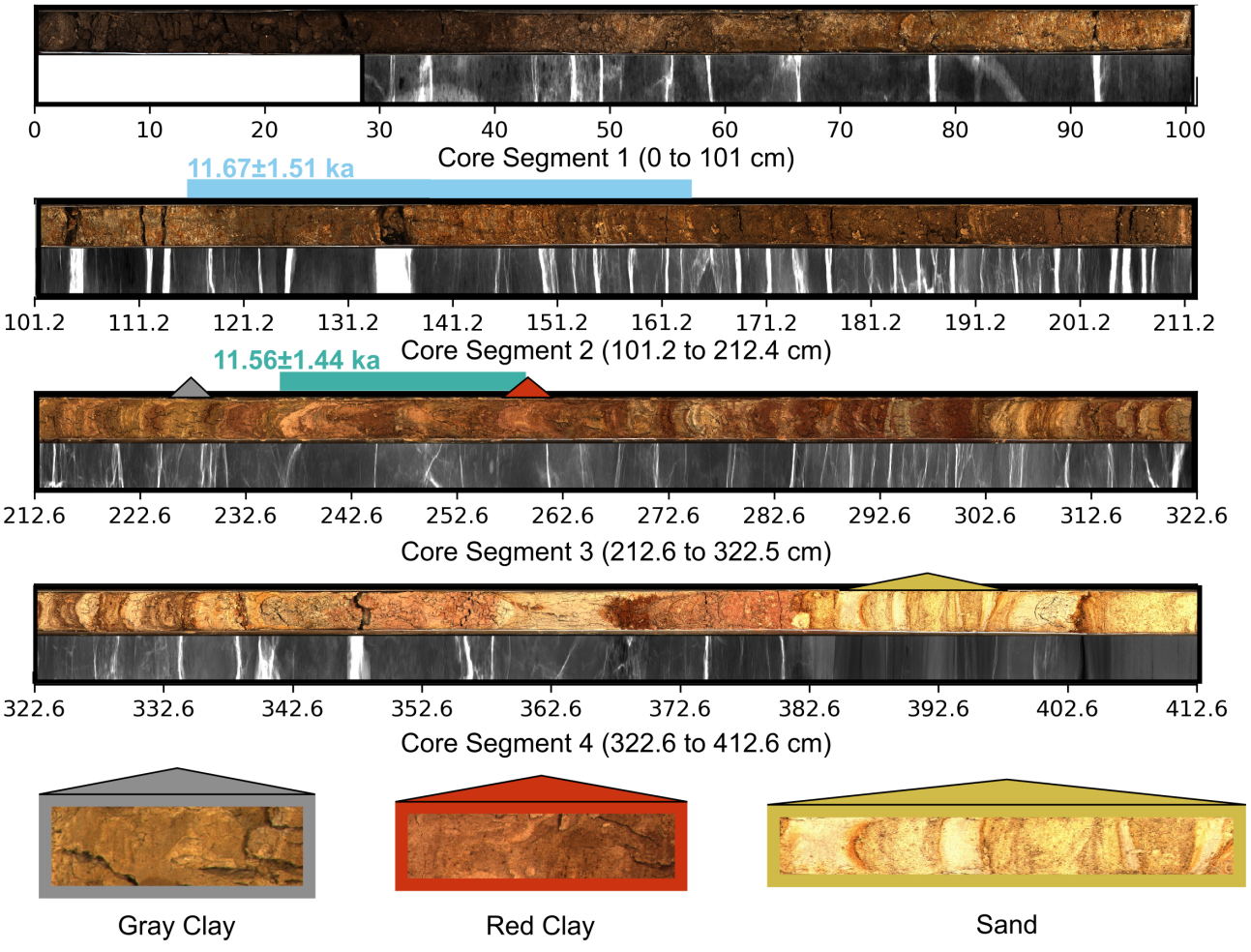

Figure 3. A) X-radiographic images (left along columns) and corresponding high-resolution image scans (right along columns) of the sediment core segments. OSL age results are indicated in light blue and teal at their corresponding sampling depths. Major lithologies are shown in insets on the right and indicated on the core segments as triangles and include gray clay (gray box and triangle), red clay (red box and triangle), and locally derived sand (yellow box and triangle). B) Stratigraphic column for core sections.

240 3; Penprase et al., 2025). From 392–382 cm, this quartz-rich sand begins to incorporate small (mm-scale) gray clay beds before fully transitioning to cm-scale red and gray clay beds (382 cm). These red and gray clay packages become quite large (occasionally >10 cm thick) as sediment continues to accumulate to 337 cm depth before transitioning to smaller, 1-cm thick red and gray clay beds with occasional lenses of sand from 337 cm up to 213 cm depth. At depths < 213 cm (corresponding to Core Segments 1 & 2) the sediments become visibly weathered, with signs of magnesium staining and possible redox reactions
245 (250–50 cm). The top of the sediment core (<40 cm) is an organic-rich soil profile (0–40 cm).

https://doi.org/10.5194/egusphere-2025-3920
Preprint. Discussion started: 19 September 2025
© Author(s) 2025. CC BY 4.0 License.

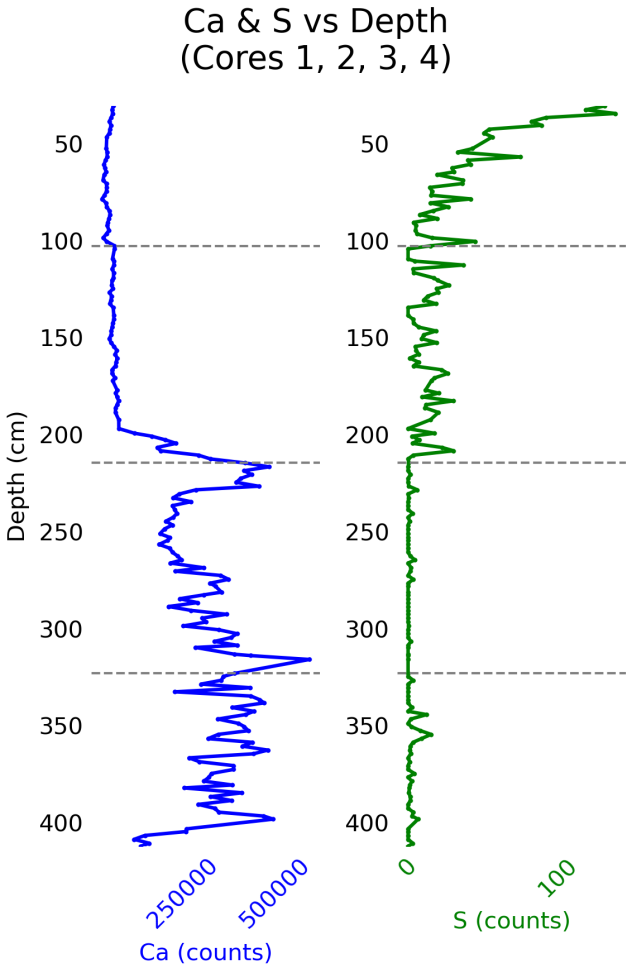

Figure 4. Ca and S concentrations for Core Segments 1–4. Dashed lines delineate different core segments. Major shift in concentration at the base of Core Segment 2 (at depths $\lesssim$200 cm) likely due to leaching and weathering. These data are, therefore, omitted from analyses and only Core Segments 3 & 4 are used.

https://doi.org/10.5194/egusphere-2025-3920
Preprint. Discussion started: 19 September 2025
© Author(s) 2025. CC BY 4.0 License.

4.3 X-Ray Fluorescence (XRF) Data and Elemental Changes with Depth

Our sediment observations of a highly weathered soil horizon in the top ∼200 cm of the sediments is further corroborated by the XRF data, as XRF shows considerably higher sulfur (S) and and considerably lower calcium (Ca) concentrations in the top 200 cm of the core (Figure 4). These changes in S and Ca can be directly tied to soil forming processes and agricultural practices, as increased S is commonly associated with decomposition in soil horizons (Schroth et al., 2007) and S is commonly added to soils to facilitate production of corn and wheat (Sharma et al., 2024). Both corn and wheat were commonly cultivated in the Whitewater River watershed following Euro-American settlement in the watershed after the 1850s C.E. (Holger, 2019). Decreased Ca concentrations further corroborate post-settlement alteration via weathering and agriculture, as loss of Ca is a common sign of leaching in soils, and the application of nitrogen (N) fertilizer to agricultural fields has been shown to greatly increase Ca leaching loss (Zhou et al., 2024). Therefore, to avoid the impact of post-depositional geochemical alteration of sediments, we focused our analyses and interpretation on sediments below this weathered horizon (>212 cm; Core Segments 3 & 4).

Plots of elemental concentration with depth for the five elements of interest below the weathered horizon (>212 cm, Figure 5) show a high amount of variability throughout the sediment core. Moving from bottom to top, Si exhibits noticeably higher concentrations in the lowermost sediments of the core (>400 cm), with lower but variable concentrations for the rest of the section of interest. Ca similarly has a small increase in concentration at lower depths (∼400 cm) and remains noticeably high in concentration from ∼400 to 300 cm, before decreasing above 300 cm until 225 cm. Fe, Cu, and Ni show high variability in concentrations as well in the lower section of the core, with large peaks for Fe and Ni at ∼360 cm before a slight increase in concentration at 300 cm (corresponding to a decrease in Ca) before decreasing slightly at depths above ∼250 cm.

4.4 Principal Component Analysis (PCA) and k-means clustering

To mitigate the impacts of post-depositional changes to geochemistry of the uppermost sediments >212 cm (Core Segments 1 & 2), our geochemical interpretations focus on depths below 212 cm (Core Segments 3 & 4), where the post-depositional alteration was no longer pervasive. The PC1 axis of the PCA (Figure 6), which drives the greatest variance in the dataset, accounts for 44.5% of variability and is forced most strongly in the positive direction by Ca (33.5%), Cu (30.0%), and Ni (24.7%). The PC2 axis accounts for 30.4% of the variability, and is most strongly driven by Fe (51.7%) and Si (41.9%). Si plots nearly orthogonally to Fe + Cu + Ni, indicating almost no correlation, while Ca and Ni plot nearly 180 degrees apart, indicating negative correlation between elements (Figure 6).

Using the elbow method to identify the optimal number of clusters (k) for the dataset, we apply k-means clustering of the dataset to identify three groupings (k=3). The resultant groupings are centered around Ca, Fe + Cu + Ni, and Si (Figure 6), which we tie to the provenance locations of Agassiz, Superior, and Local, respectively. Going forward, we refer to sediments from each region as Agassiz-group, Superior-group, and Local-group. The plot of cluster distribution with depth shows a high amount of change in the relative abundance of points from each provenance through the core. Local-group points are highly prevalent at lower depths within the core, with two large peaks at ∼410 cm and 390 cm, before tapering off by 300

https://doi.org/10.5194/egusphere-2025-3920
Preprint. Discussion started: 19 September 2025
© Author(s) 2025. CC BY 4.0 License.

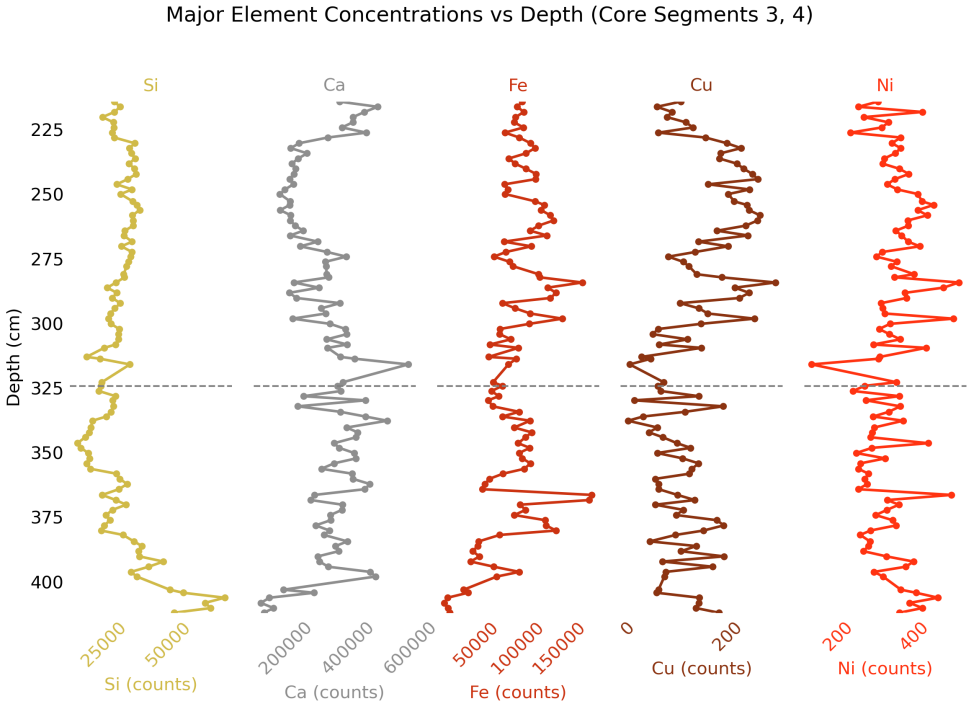

Figure 5. Major element concentrations for Si (yellow; local), Ca (gray; Agassiz), and Fe, Cu, and Ni (shades of red; Superior) within the depth interval of interest (>212 cm) averaged over 2 cm increments. Gray dashed line denotes transition from Core Segment 3 to Core Segment 4.

cm. Agassiz-group points have a more constant prevalence throughout the core, with a gradual increase in prevalence in the up-core direction that peaks at ∼350, decreases until ∼250 cm, and exhibits a small resurgence at the top of Core Segment 3. Superior-group points show a small increase in prevalence at ∼375 cm, before decreasing until a larger peak, with an initial maximum at ∼290 cm and highest prevalence at ∼250 cm. Above ∼250 cm, Superior-group elements gradually decline in prevalence with depth. We additionally place the deeper OSL sample (∼247 cm depth) on Figure 6, indicating that the highest concentration of Superior-provenance sediments correlates with an age of 11.56 ± 1.44 ka. Our shallower OSL sample (∼140 cm depth) coincides with the altered sediments in the core and is therefore not plotted with the PCA results, but overlaps in age within error (11.67 ± 1.51 ka) with the deeper OSL sample.

5 Discussion

XRF and PCA results indicate that the core predominately comprises non-local, glacial meltwater-sourced slackwater sediments. Based on shifts in dominant provenance with depth (Figures 5 & 6) we suggest a five-phase progression of shifting

https://doi.org/10.5194/egusphere-2025-3920
Preprint. Discussion started: 19 September 2025
© Author(s) 2025. CC BY 4.0 License.

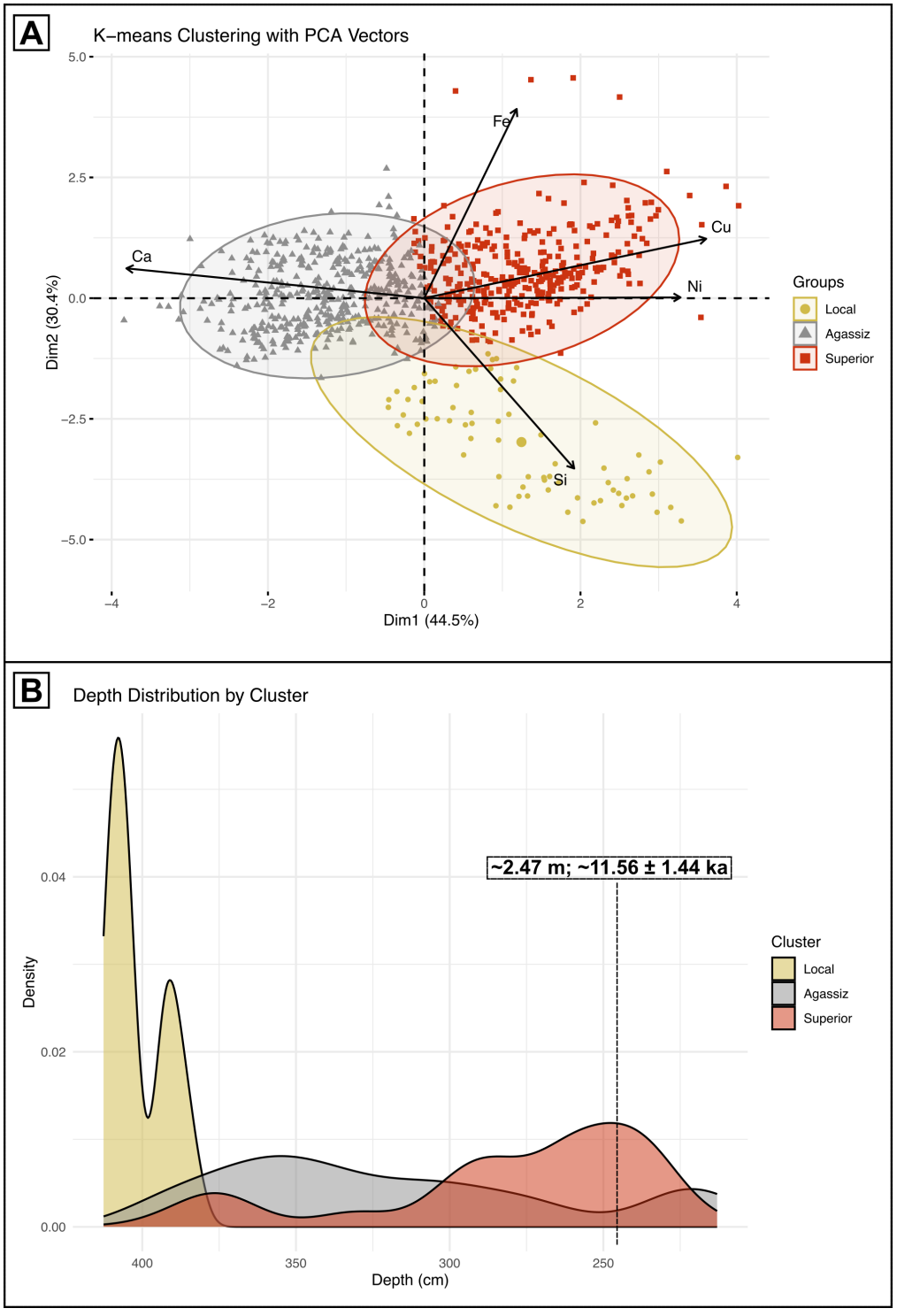

Figure 6. A) Principal component analysis (PCA) and k-means clustering of XRF data for the major elements of interest Ca (Agassiz, gray), Fe, Cu, Ni (Superior, red), and Si (local, yellow). B) Depth-dependent variability of elemental groups from k-means clustering with associated group colors. Sampling depth and associated age of our lower OSL sample indicated by dashed black line.

https://doi.org/10.5194/egusphere-2025-3920
Preprint. Discussion started: 19 September 2025
© Author(s) 2025. CC BY 4.0 License.

sediment source. In order from deepest to shallowest, these are: (1) locally derived sediments that transition to (2) NW, Agassiz basin sediments, followed by (3) mixed Superior and Agassiz-basin sediments, (4) a final transition to NE, Superior basin sediments, and (5) a cessation of glacial meltwater inputs to the upper Mississippi River Valley (Figures 6 & 7).

Based on the OSL age of ∼11.6 ka, we correlate the sedimentary sequence captured in the core to Laurentide Ice Sheet advance and retreat associated with the Marquette Readvance during the final phase of ice retreat north of the modern US-Canada border. During the Marquette Readvance, Superior Lobe ice reached its maximal extent in the upper peninsula of modern day Michigan at 10.025±0.055 ^{14}C kyr BP (Lowell et al., 1999), which we recalibrate following IntCal20 (Reimer et al., 2020) to 11.54 (+0.19, -0.21) ka. In the St. Croix River watershed, Clayton (1984) notes a correlated advance called the Lake View margin. For the remainder of this paper, we will refer to it as the Marquette Readvance. We suggest that the sediments captured in our core capture the associated sediment provenance changes from glacial meltwater drainage rerouting and alternating reactivation of NW (Agassiz) and NE (Superior) drainages triggered by Superior Lobe ice advance and retreat during the Marquette Readvance.

The five-phase chronology we identify is consistent with stratigraphy observed farther downstream along the Mississippi River. Johnson (2009) observed a similar stratigraphic sequence near Savanna, in northwestern Illinois. There, alluvium dated to 15.3 ka (12840±80 ^{14}C yr BP) and 15.6 ka (13020±45 ^{14}C yr BP) lies beneath an undated sequence of slackwater sediments whose sources (in stratigraphic order from the alluvium–slackwater contact) progressed from Agassiz to mixed and reworked glacially derived materials to a cap of Superior-derived sediments. Although Van Nest (2014) lacked the full stratigraphic sequence, the authors noted that the uppermost Slackwater sediments at Sny Bottoms, south of Quincy, Illinois, were of Lake Superior provenance and bracketed the age of their observed slackwater sediments with radiocarbon dates, establishing an age between 12.26 (+0.33, −0.23) ka (10.40±0.13 ^{14}C kyr BP) and 10.84±0.23 ka (9.51±0.08 ^{14}C kyr BP). We report these ages with 1σ age bounds (68% confidence interval). Bettis et al. (2008) further notes that this uppermost layer of sediments with Lake Superior provenance extends broadly across the Upper Mississippi River Valley.

5.1 Phase 1 (Before 13 ka): Locally derived sandy alluvium and terrace abandonment

From the PCA and k-means clustering, we find that sediments at the base of the sediment core have highly elevated concentrations of Si (Figure 6). We associate this high concentration of Si with dominant local inputs: quartz grains sourced from local sandstone bedrock comprise aggradational sandy alluvial deposits within the Whitewater River during a period of no tributary inundation along the Upper Mississippi River Valley (Figure 7A). While both Si concentration and grain size increase in the lower ∼20 cm of the sediment core, we attribute this change to a change in sediment source, rather than an increase triggered by grain size alone, as the sediments in this interval are markedly different than all other fine-grained, red and gray clay species found within in the core segments (Figure 3). Furthermore, these grains are highly similar to local, alluvial sediments sourced from the sandstone bedrock that underlies much of the catchment (Penprase et al., 2025; Runkel, 1996). Thus, while Si is present in some capacity in all glacially sourced sediments due to the high concentrations of Si in continental crust (Rudnick and Gao, 2003), we attribute the anomalously high concentrations in Si at the base of the core segment to elevated local sediment input. Additionally, based on the textural and geochemical differences between this local, sandy alluvium captured at the

https://doi.org/10.5194/egusphere-2025-3920
Preprint. Discussion started: 19 September 2025
© Author(s) 2025. CC BY 4.0 License.

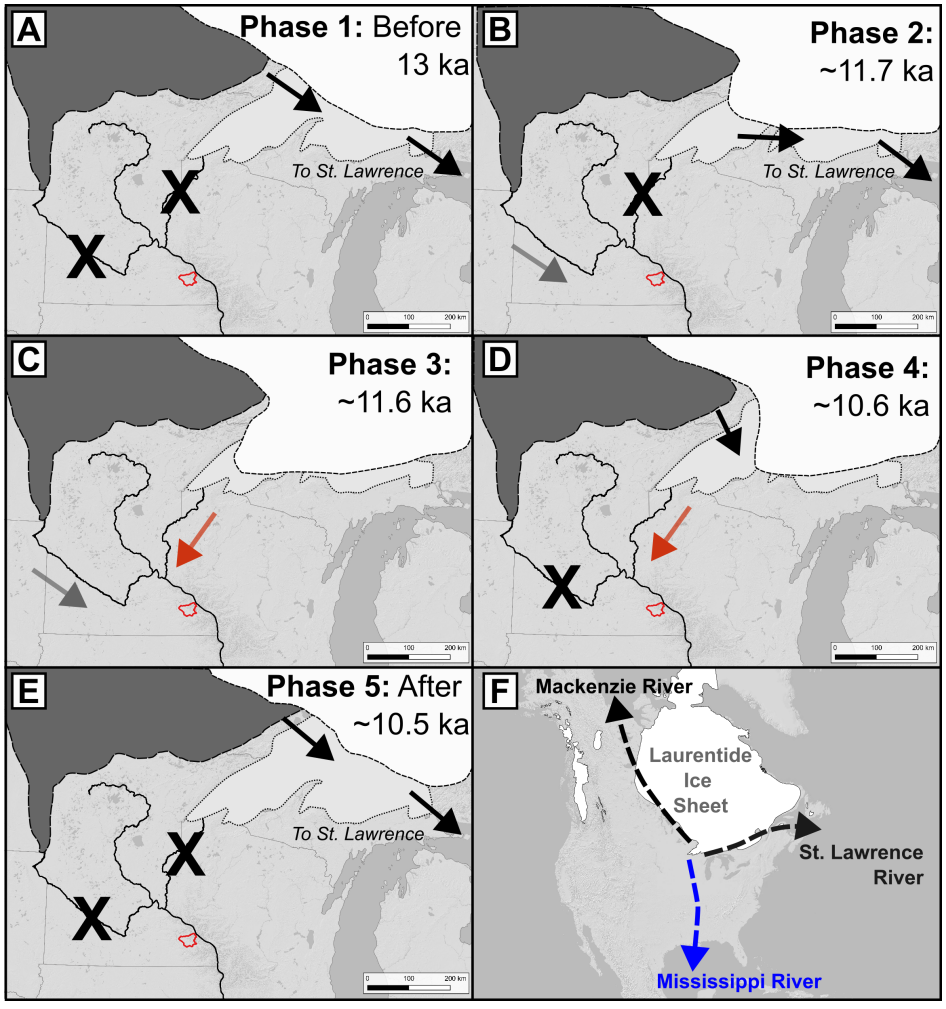

Figure 7. A-E) Proposed meltwater routing based on the core sediments and available literature. Arrows indicate direction of meltwater routing, with Agassiz-basin arrow colored gray and the Superior-basin arrow colored red to match provenance sediment color. X's indicate no glacial meltwater inputs at that time interval. F) Possible Laurentide Ice Sheet meltwater routes for Glacial Lake Agassiz and Superior Basins (Süfke et al., 2022; Wickert et al., 2023) and the 11.5 ka ice margin (Dalton et al., 2023). Each of these major drainage pathways was active at variable intervals during the last deglaciation, not necessarily at 11.5 ka.

https://doi.org/10.5194/egusphere-2025-3920
Preprint. Discussion started: 19 September 2025
© Author(s) 2025. CC BY 4.0 License.

base of the core segment and the clay-rich beds in the rest of the sediment core, we conclude that the majority of the sediment core segments comprises non-local sediments derived from proglacial river systems.

Locally derived fluvial sediments at the base of the core segment (Figure 7) correlate with those atop the Savanna Terrace of the Mississippi River (Penprase, 2024). Geochronological data on the Savanna Terrace indicate that the Mississippi River incised and abandoned it as an active floodplain between 18 ka (Bettis et al., 2008; Knox, 2007) and 13 ka (Wickert et al., 2024), with the latter ages corresponding to meltwater floods from glacial Lake Agassiz (approx. 13.4 ka; Lepper et al. (2013);7. Thus, these core sediments were likely deposited as part of this Savanna Terrace surface that was subsequently abandoned before being overtopped by the glacial meltwater pulses that deposited the rest of the core.

The interval between Savanna terrace abandonment and a return to meltwater inundation down the upper Mississippi River Valley was marked by a number of shifts in spillway activation throughout the deglacial period, with intervals of meltwater delivery and intervals without (Wickert et al., 2023). By ca. 12.9–12.8 ka, the Upper Mississippi River Valley was not receiving glacial meltwater and outflow had been rerouted to the north via the Mackenzie River and east via the St. Lawrence River (Fisher, 2003; Murton et al., 2010; Leydet et al., 2018; Keigwin et al., 2018; Wickert et al., 2023). This timing is supported by a range of regional and more distant data: marine cores from the Beaufort Sea indicate continued input of meltwater to the NW and the Mackenzie delta from ∼12.85 to 12.35 ka (Keigwin et al., 2018) and excess meltwater routing eastwards through the eastern Great Lakes and St. Lawrence outlets at ∼12.6 to 12.7 ka (Carlson et al., 2007). Additionally, cosmogenic nuclide dates from the eastern outlet of Agassiz into the Superior basin suggest active flow at 12.7 ± 0.3 ka (Leydet et al., 2018). Finally, Young et al. (2021) generated a compilation of Glacial Lake Agassiz water levels and found an onset range of ∼12.41 for the Moorhead low-water phase. This phase is traditionally associated with Agassiz outflow to the east toward the Superior basin (Young et al., 2021; Lepper et al., 2013; Leydet et al., 2018). This interval without meltwater delivery to the Mississippi River presumably led to a time of post-incision floodplain stabilization and river aggradation (Knox, 2007; Bettis and Mandel, 2002). Despite this re-aggradation of the incised valley, the floodplain remained below the level of the Savanna terrace. As a result, prior to ice-sheet readvance, only an exceptionally large flood could create high enough water to inundate the Savanna Terrace and initiate renewed floodplain deposition.

5.2 Phase 2 (∼11.7 ka): Glacial Lake Agassiz via Glacial River Warren

Moving up stratigraphy in our sediment core, above 400 cm local inputs largely disappear and, instead, sediments from the NW (Agassiz) provenance become most prevalent, with a small increase in Superior sediments at ∼375 cm, that remains below the high occurance of Agassiz-basin sourced sediments within this interval (Figure 6). We associate this elevated Agassiz input with the initial pulse of Glacial Lake Agassiz-derived meltwater down a reactivated Glacial River Warren (NW; Figure 7) following the initiation of the Marquette Readvance. Starting ∼11.7 ka, ice from the Marquette Readvance began to fill the Superior Basin and blocked eastern drainage of Lake Agassiz into the Superior Basin (Fisher and Smith, 1994; Lowell et al., 1999) and triggered reactivation of Lake Agassiz' southern drainage via Glacial River Warren (Fisher, 2003). Evidence for the timing of this advance comes from a transition towards isotopically light, and therefore likely glacially sourced, meltwater reaching the

https://doi.org/10.5194/egusphere-2025-3920
Preprint. Discussion started: 19 September 2025
© Author(s) 2025. CC BY 4.0 License.

Gulf of Mexico during this interval (Wickert et al., 2023). Within the bounds of local age constraints, this meltwater rerouting also corresponds to the lower slackwater sediments observed by Johnson (2009) and Van Nest (2014).

5.3 Phase 3 (∼11.6 ka): Mixed sediments from Glacial Lake Agassiz and the Superior Basin via both routing pathways

After 350 cm depth, Agassiz sediments gradually decrease, while Superior sediments begin to rise. By 290 cm depth, the prevalence of NW (Agassiz) and NE (Superior) sediments in the core are equal. We suggest that this interval in the sediment core preserves a period when both NW (Agassiz) and NE (Superior) drainages were active glacial meltwater pathways. As Marquette-phase ice continued to advance, the ice lobe blocked eastward drainage of the Lake Superior to the Atlantic via the Great Lakes and the St. Lawrence River. This rerouted outflow from the Superior Basin southwards (Wickert, 2016; Wickert et al., 2023), reactivating the Glacial St. Croix River and leading to a period where Glacial River Warren and the Glacial St Croix River both actively delivered glacial meltwater to the Upper Mississippi River Valley. The start of this phase likely predates the burial and subsequent ice advance across the Lake Gribben Forest bed, which marks advance of Superior Lobe ice onto the southern shore of modern-day Lake Superior. Lowell et al. (1999) radiocarbon dated in-situ wood from this buried forest and statistically combined these ages to obtain a bulk age estimate of 10.025 ± 0.055 ^{14}C kyr BP to constrain ice advance, which we recalibrate to 11.54 (+0.19, -0.21) ka (Reimer et al., 2020).

5.4 Phase 4 (∼10.6 ka): Superior Basin sediments via the Glacial St. Croix

Following the 290-cm interval where both provenances are equally present in the dataset, NE, Superior-sourced sediments become the most common, with an increase at ∼290 cm. While this second peak in NE, Superior sediments coincides with the depth of the lowermost OSL sample (11.56 ka ± 1.44 ka), we believe the true age of these sediments lie on the younger end of the error bounds and tie this period of larger Superior inputs to Marquette Readvance retreat. We suggest that ongoing Marquette Readvance ice retreat after ∼10.6 ka would have reopened Lake Agassiz drainage pathways to the Lake Superior basin. This age is recorded by three sets of thick–thin varves in the Western Lake Superior basin, which may be interpreted to indicate progressive floods of water from Lake Agassiz into Lake Superior (Breckenridge, 2007). While Lake Agassiz waters were able to flow into the Superior Basin, we propose that the eastern outlets of Lake Superior remained closed by ice. The eastern Superior outlets remaining closed permitted the combined waters to traverse the western Superior Basin (Glacial Lake Duluth) and drain through the Moose Lake/Portage outlet and later the Brule outlet into the St. Croix River valley. This shift would have greatly diminished meltwater delivery to the Upper Mississippi River Valley via Glacial River Warren and would have instead resulted in a dominant NE, Superior basin signal in glacially sourced meltwater at this time consistent with our slackwater data (Figure 7).

https://doi.org/10.5194/egusphere-2025-3920
Preprint. Discussion started: 19 September 2025
© Author(s) 2025. CC BY 4.0 License.

5.5 Phase 5 (After ∼10.5 ka): Cessation of glacial meltwater inputs to the Upper Mississippi River

Because of we focus our analysis on only Core Segments 3 and 4, to avoid post-depositional alteration in sediments above ∼200 cm depth in Core Segments 1 and 2, we are not able to directly relate shifts in sediment geochemistry to glacial meltwater sourcing sediments for the uppermost sediments captured in Core Segments 1 and 2. However, downstream observations by Van Nest (2014) noted a red-brown cap of fine-grained, slackwater sediments along the Mississippi River in western Illinois and attributed the topmost slackwater sediments to a Superior-basin source. Based on local stratigraphic relationships and geochronology, these Superior-basin sourced sediments were deposited sometime after ∼12.3 ka (10,400 ± 130 ^{14}C yr BP) but before ∼10.8 ka (9,490 ± 140 ^{14}C yr BP) (Van Nest, 2014; Bettis et al., 1992), suggesting that sediments within top meters of our core are likely Superior in origin. The modern Whitewater River occupies a floodplain 20 m below the surface where our sediment core segments were taken and previous studies of non-slackwater terraces in the Whitewater place the lowermost regional terrace elevation abandonment at ∼10.6 ka (7.3 – 13.7 ka; Penprase et al., 2025). Additionally, prior work (e.g., Breckenridge, 2013) has noted that an eastward routing of meltwater in the Superior Basin occurred when Glacial Lake Duluth and Glacial Lake Minong merged as Marquette-phase ice retreated north. This has been reinforced by current work (Fischer et al., 2024) suggesting a high-magnitude rerouting event shifting meltwater drainage eastward in the Superior Basin around 10.5 – 10.6 ka. Ultimately, this would have shut of meltwater delivery to the Upper Mississippi River Valley and is consistent with ages from basal sediments within the lower St. Croix and upper Mississippi (Blumentritt et al., 2009). Therefore, we propose the top sediments in our core capture the continued Marquette Readvance ice retreat identified in previous studies. This reopening would have resulted in a final end of glacial meltwater delivery to the Upper Mississippi River Valley and the cessation of slackwater sediment deposition along the Upper Mississippi River Valley and the mouths of its tributaries (Figure 7; (Breckenridge and Johnson, 2009; Wickert et al., 2023; Van Nest, 2014).

6 Conclusion

Results of this study provide a new, detailed record of the most recent glacially derived slackwater deposition along the Upper Mississippi River Valley. The proposed meltwater routing chronology directly ties slackwater sediments delivered to the Upper Mississippi River Valley to their sources from ∼11.7–10.6 ka and is associated with glacial meltwater rerouting triggered by the Marquette Readvance within the Superior Basin. Our stratigraphically grounded sequence begins with locally derived fluvial sands that are overlain by northwesterly sourced slackwater sediments, carried by Glacial River Warren from the Lake Agassiz region as advancing ice during the Marquette Readvance Agassiz drainage southward. These sediments are overlain by mixed NE/NW-sourced sediments from both Lake Agassiz and the Superior Basin during the period of ice pullback, as both spillways became active. The sequence is capped by northeasterly sourced Superior Basin sediments, routed to the Mississippi via the St. Croix River as ice retreat following the Marquette Readvance reopened eastward Agassiz drainage. While post-depositional alteration of the uppermost sediments in the uppermost core segments inhibit the ability to link these sediment to their source, slackwater deposition almost certainly ceased by 10.5ka due to the cessation of meltwater delivery to the Upper Mississippi River Valley and eastward rerouting of meltwater via both Lake Agassiz and Lake Superior. Our findings place new constraints

https://doi.org/10.5194/egusphere-2025-3920
Preprint. Discussion started: 19 September 2025
© Author(s) 2025. CC BY 4.0 License.

on the evolution of Marquette Readvance phase ice during the final phases of Laurentide Ice Sheet meltwater delivery to the Upper Mississippi River Valley at the earliest Holocene.

Data availability. All optically stimulated luminescence data is provided in the tables and figures and in the Supplement. Glacial lake and river shapefiles in Figures 1 & 7 are adapted from Dyke (2004). Ice margin in Figure 7 is from Dalton et al. (2023). Minnesota state soil geochemistry data used in Figure 2 and described in the text was downloaded at https://hdl.handle.net/11299/117364 (Lively and Thorleifson, 2009). High resolution core images, X-radiographic images, and X-Ray Fluorescence data are available at https://doi.org/10.5281/zenodo.16779577 (Penprase et al., 2025).

Author contributions. SBP, ADW, and PHL conceived the study. PHL completed initial field reconnaissance and discovered the sediment deposits. SBP and ADW collected field samples. SBP and TR analyzed OSL samples. SBP and ACW completed sediment description, core segment imaging, and XRF laboratory analysis. ACW, ADW, and PHL assisted SBP in literature review. MM helped with generation and interpretation of PCA plots. SBP processed the data, generated the figures, and wrote the manuscript with input from all authors.

Competing interests. The authors declare no competing interests.

Acknowledgements. This material is based upon work supported by the United States National Science Foundation under Grant Nos. 1944782 and 2218457. Initial core segment imaging performed at the Continental Scientific Drilling Facility, University of Minnesota. XRF analysis was completed at the Large Lakes Observatory by R. Brown. C. Dunn assisted in initial core processing and description. G. Running, D. Faulkner, J. Jones, C. Dunn, J. Kwang, H. Hassenruck-Gudipati, T. Fulgham, and P. Mitchell helped in the field. K. Lutz provided statistical analysis support and M. Romero assisted with manuscript formatting.

https://doi.org/10.5194/egusphere-2025-3920
Preprint. Discussion started: 19 September 2025
© Author(s) 2025. CC BY 4.0 License.

References

Bettis, E., Baker, R., Green, W., Whelan, M., and Benn, D.: Late Wisconsinan and Holocene alluvial stratigraphy, paleoecology, and archaeological geology of east-central Iowa, Tech. rep., Iowa Department of Natural Resources, Iowa City, IA, 1992.

Bettis, E. A. and Mandel, R. D.: The effects of temporal and spatial patterns of Holocene erosion and alluviation on the archaeological record of the Central and Eastern Great Plains, U.S.A., Geoarchaeology, 17, 141–154, https://doi.org/10.1002/gea.10006, 2002.

Bettis, E. A., Benn, D. W., and Hajic, E. R.: Landscape evolution, alluvial architecture, environmental history, and the archaeological record of the Upper Mississippi River Valley, Geomorphology, 101, 362–377, https://doi.org/10.1016/j.geomorph.2008.05.030, 2008.

Blumentritt, D. J., Wright, H. E., and Stefanova, V.: Formation and early history of Lakes Pepin and St. Croix of the upper Mississippi River, Journal of Paleolimnology, 41, 545–562, https://doi.org/10.1007/s10933-008-9291-6, 2009.

Breckenridge, A.: The Lake Superior varve stratigraphy and implications for eastern Lake Agassiz outflow from 10,700 to 8900 cal ybp (9.5–8.0 14C ka), Palaeogeography, Palaeoclimatology, Palaeoecology, 246, 45–61, https://doi.org/10.1016/j.palaeo.2006.10.026, 2007.

Breckenridge, A.: An analysis of the late glacial lake levels within the western Lake Superior basin based on digital elevation models, Quaternary Research, 80, 383–395, https://doi.org/10.1016/j.yqres.2013.09.001, 2013.

Breckenridge, A. and Johnson, T. C.: Paleohydrology of the upper Laurentian Great Lakes from the late glacial to early Holocene, Quaternary Research, 71, 397–408, https://doi.org/10.1016/j.yqres.2009.01.003, 2009.

Breckenridge, A., Lowell, T., Peteet, D., Wattrus, N., Moretto, M., Norris, N., and Dennison, A.: A new glacial varve chronology along the southern Laurentide Ice Sheet that spans the Younger Dryas–Holocene boundary, Geology, 49, 283–288, https://doi.org/10.1130/G47995.1, 2021.

Carlson, A. E., Clark, P. U., Haley, B. A., Klinkhammer, G. P., Simmons, K., Brook, E. J., and Meissner, K. J.: Geochemical proxies of North American freshwater routing during the Younger Dryas cold event, Proceedings of the National Academy of Sciences, 104, 6556–6561, https://doi.org/10.1073/pnas.0611313104, 2007.

Carson, E. C.: Late MIS3 onset to large-scale Aggradation on the Upper Mississippi River Valley, USA, in: Fluvial Responses to Perturbations at Varying Spatial and Temporal Scales I, Geological Society of America Abstracts with Programs, Phoenix, AZ, https://doi.org/10.1130/abs/2019AM-334287, 2019.

Carson, E. C., Rawling, J. E., and Attig, J. W.: The glacial record in regions surrounding the Driftless Area, The Physical Geography and Geology of the Driftless Area: The Career and Contributions of James C. Knox, pp. 37–50, https://doi.org/10.1130/2019.2543(02), 2019.

Clark, P. U., Dyke, A. S., Shakun, J. D., Carlson, A. E., Clark, J., Wohlfarth, B., Mitrovica, J. X., Hostetler, S. W., and McCabe, A. M.: The Last Glacial Maximum, Science, 325, 710–714, https://doi.org/10.1126/science.1172873, 2009.

Clayton, L.: Pleistocene Geology of the Superior Region, Wisconsin, Information Circular IC46, Wisconsin Geological and Natural History Survey, https://doi.org/10.54915/fdmm3282, series: Information Circular, 1984.

Condron, A. and Winsor, P.: Meltwater routing and the Younger Dryas, Proceedings of the National Academy of Sciences, 109, 19 928–19 933, https://doi.org/10.1073/pnas.1207381109, 2012.

Costa, S., Sidky, H., and Creel, R.: IOSACal: v0.6.0, https://doi.org/10.5281/zenodo.7133343, 2022.

Curry, B. B. and Grimley, D. A.: Provenance, age, and environment of mid-wisconsinan slackwater lake sediment in the St. Louis Metro East Area, USA, Quaternary Research, 65, 108–122, https://doi.org/10.1016/j.yqres.2005.09.005, 2006.

https://doi.org/10.5194/egusphere-2025-3920
Preprint. Discussion started: 19 September 2025
© Author(s) 2025. CC BY 4.0 License.

Dalton, A. S., Dulfer, H. E., Margold, M., Heyman, J., Clague, J. J., Froese, D. G., Gauthier, M. S., Hughes, A. L., Jennings, C. E., Norris, S. L., and Stoker, B. J.: Deglaciation of the north American ice sheet complex in calendar years based on a comprehensive database of chronological data: NADI-1, Quaternary Science Reviews, 321, 108 345, https://doi.org/10.1016/j.quascirev.2023.108345, 2023.

Durcan, J. A., King, G. E., and Duller, G. A.: DRAC: Dose Rate and Age Calculator for trapped charge dating, Quaternary Geochronology, 28, 54–61, https://doi.org/10.1016/j.quageo.2015.03.012, 2015.

Dyke, A. S.: An outline of North American deglaciation with emphasis on central and northern Canada, Developments in Quaternary Science, 2, 373–424, https://doi.org/10.1016/S1571-0866(04)80209-4, 2004.

Faulkner, D. J., Larson, P. H., Jol, H. M., Running, G. L., Loope, H. M., and Goble, R. J.: Autogenic incision and terrace formation resulting from abrupt late-glacial base-level fall, lower Chippewa River, Wisconsin, USA, Geomorphology, 266, 75–95, https://doi.org/10.1016/j.geomorph.2016.04.016, publisher: Elsevier B.V., 2016.

Fischer, A., Susnik, C., Stafford, N., Delikowski, H., Rowen, J., Breckenridge, A., Larson, P., Seong, Y. B., Faulkner, D., Ullman, D., Wickert, A., Barefoot, E., and Brown, A.: A Sedimentologic, Morphometric, and Geochronologic Investigation of Ambiguous Dune-like Landforms: An Indicator of Proglacial Lake Drainage in the Lake Superior Basin, USA, Tech. Rep. EGU24-4108, Copernicus Meetings, https://doi.org/10.5194/egusphere-egu24-4108, conference Name: EGU24, 2024.

Fisher, T. G.: Chronology of glacial Lake Agassiz meltwater routed to the Gulf of Mexico, Quaternary Research, 59, 271–276, https://doi.org/10.1016/S0033-5894(03)00011-5, 2003.

Fisher, T. G.: Megaflooding associated with glacial Lake Agassiz, Earth-Science Reviews, 201, 102 974, https://doi.org/10.1016/j.earscirev.2019.102974, 2020.

Fisher, T. G. and Breckenridge, A.: Relative lake level reconstructions for glacial Lake Agassiz spanning the Herman to Campbell levels, Quaternary Science Reviews, 294, 107 760, https://doi.org/10.1016/j.quascirev.2022.107760, 2022.

Fisher, T. G. and Smith, D. G.: Glacial Lake Agassiz: Its northwest maximum extent and outlet in Saskatchewan (Emerson Phase), Quaternary Science Reviews, 13, 845–858, https://doi.org/10.1016/0277-3791(94)90005-1, 1994.

Flock, M. A.: The late Wisconsinan Savanna Terrace in tributaries to the upper Mississippi River, Quaternary Research, 20, 165–176, https://doi.org/10.1016/0033-5894(83)90075-3, 1983.

Galbraith, R. and Roberts, R.: Statistical aspects of equivalent dose and error calculation and display in OSL dating: An overview and some recommendations, Quaternary Geochronology, 11, 1–27, https://doi.org/10.1016/j.quageo.2012.04.020, 2012.

Gran, K., Finnegan, N., Johnson, A., Belmont, P., Wittkop, C., and Rittenour, T.: Landscape evolution, valley excavation, and terrace development following abrupt postglacial base-level fall, Geological Society of America Bulletin, 2013.

Guérin, G., Mercier, N., and Adamiec, G.: Dose-rate conversion factors: update, Ancient TL, 29, 2011.

Holger, S.: Whitewater State Park: 100 Years in Paradise, Open Rivers: Rethinking Water, Place & Community, p. 9, https://openrivers.lib.umn.edu/article/whitewater-state-park/, 2019.

Ivanovic, R. F., Gregoire, L. J., Burke, A., Wickert, A. D., Valdes, P. J., Ng, H. C., Robinson, L. F., McManus, J. F., Mitrovica, J. X., Lee, L., and Dentith, J. E.: Acceleration of Northern Ice Sheet Melt Induces AMOC Slowdown and Northern Cooling in Simulations of the Early Last Deglaciation, Paleoceanography and Paleoclimatology, 33, 807–824, https://doi.org/10.1029/2017PA003308, 2018.

Johnson, B.: Provenance of Slackwater Sediments in the Savanna Terrace, Northwestern Illinois, Doctoral Thesis, Northern Illinois University, De Kalb, Illinois, 2009.

Karrow, P. F., Dreimanis, A., and Barnett, P. J.: A Proposed Diachronic Revision of Late Quaternary Time-Stratigraphic Classification in the Eastern and Northern Great Lakes Area, Quaternary Research, 54, 1–12, https://doi.org/10.1006/qres.2000.2144, 2000.

https://doi.org/10.5194/egusphere-2025-3920
Preprint. Discussion started: 19 September 2025
© Author(s) 2025. CC BY 4.0 License.

Keigwin, L. D., Klotsko, S., Zhao, N., Reilly, B., Giosan, L., and Driscoll, N. W.: Deglacial floods in the Beaufort Sea preceded Younger Dryas cooling, Nature Geoscience, 11, 599–604, https://doi.org/10.1038/s41561-018-0169-6, 2018.

Knox, J. C.: Late Quaternary Upper Mississippi River alluvial episodes and their significance to the Lower Mississippi River system, Engineering Geology, 45, 263–285, https://doi.org/10.1016/S0013-7952(96)00017-8, 1996.

Knox, J. C.: The Mississippi River System, in: Large Rivers: Geomorphology and Management, vol. 8, John Wiley & Sons, Ltd., ISBN 978-0-470-84987-3, https://doi.org/10.1080/00221340208985480, publication Title: Large Rivers: Geomorphology and Management Issue: 8 ISSN: 17526868, 2007.

Lepper, K., Buell, A. W., Fisher, T. G., and Lowell, T. V.: A Chronology for glacial Lake Agassiz shorelines along Upham's namesake transect, Quaternary Research, 80, 88–98, https://doi.org/10.1016/j.yqres.2013.02.002, 2013.

Leydet, D. J., Carlson, A. E., Teller, J. T., Breckenridge, A., Barth, A. M., Ullman, D. J., Sinclair, G., Milne, G. A., Cuzzone, J. K., and Caffee, M. W.: Opening of glacial Lake Agassiz's eastern outlets by the start of the Younger Dryas cold period, Geology, 46, 155–158, https://doi.org/10.1130/G39501.1, 2018.

Licciardi, J. M., Teller, J. T., and Clark, P. U.: Freshwater routing by the Laurentide Ice Sheet during the last deglaciation, in: Geophysical Monograph Series, vol. 112, pp. 177–201, American Geophysical Union, Washington, D. C., ISBN 978-0-87590-095-7, https://doi.org/10.1029/GM112p0177, 1999.

Lively, R. S. and Thorleifson, L. H.: OFR09-02, Minnesota Soil, Till, and Ground-Water Geochemical Data, https://hdl.handle.net/11299/117364, publisher: Minnesota Geological Survey, 2009.

Lowell, T. V., Larson, G. J., Hughes, J. D., and Denton, G. H.: Age verification of the Lake Gribben forest bed and the Younger Dryas Advance of the Laurentide Ice Sheet, Canadian Journal of Earth Sciences, 36, 1999.

Muller, E. H. and Calkin, P. E.: Timing of Pleistocene glacial events in New York State, Canadian Journal of Earth Sciences, 30, 1829–1845, https://doi.org/10.1139/e93-161, 1993.

Murray, A. S. and Wintle, A. G.: Luminescence dating of quartz using an improved single- aliquot regenerative-dose protocol, Radiation Measurements, 32, 57–73, 2000.

Murton, J. B., Bateman, M. D., Dallimore, S. R., Teller, J. T., and Yang, Z.: Identification of Younger Dryas outburst flood path from Lake Agassiz to the Arctic Ocean, Nature, 464, 740–743, https://doi.org/10.1038/nature08954, 2010.

Penprase, S. B.: Sediment, Water, Change: Post-glacial to post-agricultural evolution of river systems in the Upper Mississippi River Valley, Doctoral Thesis, University of Minnesota, Minneapolis, 2024.

Penprase, S. B., Wickert, A. D., Larson, P. H., Wood, J. J., Larsen, I. J., and Rittenour, T. M.: Plow versus Ice Age: Erosion rate variability from glacial–interglacial climate change is an order of magnitude lower than agricultural erosion in the Upper Mississippi River Valley, USA, Geology, 53, 535–539, https://doi.org/10.1130/G52585.1, 2025.

Reimer, P. J., Austin, W. E. N., Bard, E., Bayliss, A., Blackwell, P. G., Bronk Ramsey, C., Butzin, M., Cheng, H., Edwards, R. L., Friedrich, M., Grootes, P. M., Guilderson, T. P., Hajdas, I., Heaton, T. J., Hogg, A. G., Hughen, K. A., Kromer, B., Manning, S. W., Muscheler, R., Palmer, J. G., Pearson, C., Van Der Plicht, J., Reimer, R. W., Richards, D. A., Scott, E. M., Southon, J. R., Turney, C. S. M., Wacker, L., Adolphi, F., Büntgen, U., Capano, M., Fahrni, S. M., Fogtmann-Schulz, A., Friedrich, R., Köhler, P., Kudsk, S., Miyake, F., Olsen, J., Reinig, F., Sakamoto, M., Sookdeo, A., and Talamo, S.: The IntCal20 Northern Hemisphere Radiocarbon Age Calibration Curve (0–55 cal kBP), Radiocarbon, 62, 725–757, https://doi.org/10.1017/RDC.2020.41, 2020.

Ridge, J. C.: Shed Brook Discontinuity and Little Falls Gravel: Evidence for the Erie interstade in central New York, Geological Society of America Bulletin, 109, 652–665, https://doi.org/10.1130/0016-7606(1997)109<0652:SBDALF>2.3.CO;2, 1997.

https://doi.org/10.5194/egusphere-2025-3920
Preprint. Discussion started: 19 September 2025
© Author(s) 2025. CC BY 4.0 License.

Rudnick, R. L. and Gao, S.: Composition of the Continental Crust, in: The Crust, vol. 3 of *Treatise on Geochemistry*, pp. 1–64, Elsevier-Pergamon, Oxford, 2003.

Runkel, A. C.: The Geology of Whitewater State Park, Tech. Rep. Series 9, University of Minnesota, 1996.

Schroth, A. W., Bostick, B. C., Graham, M., Kaste, J. M., Mitchell, M. J., and Friedland, A. J.: Sulfur species behavior in soil organic matter during decomposition, Journal of Geophysical Research: Biogeosciences, 112, 2007JG000 538, https://doi.org/10.1029/2007JG000538, 2007.

Sharma, R. K., Cox, M. S., Oglesby, C., and Dhillon, J. S.: Revisiting the role of sulfur in crop production: A narrative review, Journal of Agriculture and Food Research, 15, 101 013, https://doi.org/10.1016/j.jafr.2024.101013, 2024.

Sionneau, T., Bout-Roumazeilles, V., Flower, B., Bory, A., Tribovillard, N., Kissel, C., Van Vliet-Lanoë, B., and Montero Serrano, J.: Provenance of freshwater pulses in the Gulf of Mexico during the last deglaciation, Quaternary Research, 74, 235–245, https://doi.org/10.1016/j.yqres.2010.07.002, 2010.

Stuiver, M. and Reimer, P. J.: Extended 14C Data Base and Revised CALIB 3.0 14C Age Calibration Program, Radiocarbon, 35, 215–230, https://doi.org/10.1017/S0033822200013904, 1993.

Süfke, F., Gutjahr, M., Keigwin, L. D., Reilly, B., Giosan, L., and Lippold, J.: Arctic drainage of Laurentide Ice Sheet meltwater throughout the past 14,700 years, Communications Earth & Environment, 3, 98, https://doi.org/10.1038/s43247-022-00428-3, 2022.

Thorleifson, L. H., Harris, K. L., Hobbs, H. C., Jennings, C. E., Knaeble, A. R., Lively, R. S., Lusardi, B. A., and Meyer, G. N.: OFR 07-01, Till geochemical and indicator mineral reconnaissance of Minnesota, Tech. rep., Minnesota Geological Survey, https://hdl.handle.net/11299/123358, publisher: Minnesota Geological Survey, 2007.

Upham, W.: Glacial Lakes in Canada, GSA Bulletin, 2, 243–276, https://doi.org/10.1130/GSAB-2-243, 1891.

Van Nest, J.: Holocene Mississippi River floods and geoarchaeological site formation processes in the Sny Bottom, western Illinois, USA, Quaternary International, 342, 114–138, https://doi.org/10.1016/j.quaint.2014.05.031, 2014.

Wickert, A. D.: Reconstruction of North American drainage basins and river discharge since the Last Glacial Maximum, Earth Surface Dynamics, 4, 831–869, https://doi.org/10.5194/esurf-4-831-2016, 2016.

Wickert, A. D., Mitrovica, J. X., Williams, C., and Anderson, R. S.: Gradual demise of a thin southern Laurentide ice sheet recorded by Mississippi drainage, Nature, 502, 668–671, https://doi.org/10.1038/nature12609, 2013.

Wickert, A. D., Williams, C., Gregoire, L. J., Callaghan, K. L., Ivanović, R. F., Valdes, P. J., Vetter, L., and Jennings, C. E.: Marine-Calibrated Chronology of Southern Laurentide Ice Sheet Advance and Retreat: ∼2,000-Year Cycles Paced by Meltwater–Climate Feedback, Geophysical Research Letters, 50, e2022GL100 391, https://doi.org/10.1029/2022GL100391, 2023.

Wickert, A. D., Clubb, F. J., Larson, P., Riedesel, S., Peffeköver, A., Penprase, S. B., Rittenour, T. M., Barefoot, E. A., Wood, J., Kuchta, M., Mitchell, P., Hassenruck-Gudipati, H. J., Jones, J., Larsen, I. J., Glade, I., Kurak, E., Schirmer, R., and Jennings, C. E.: Meltwater Floods and Isostatic Adjustment Shaped the Upper Mississippi Valley, vol. 2024, pp. EP13B–1345, https://ui.adsabs.harvard.edu/abs/2024AGUFMEP13B1345W, aDS Bibcode: 2024AGUFMEP13B1345W, 2024.

Williams, C., Flower, B. P., and Hastings, D. W.: Seasonal Laurentide Ice Sheet melting during the "Mystery Interval" (17.5–14.5 ka), Geology, 40, 955–958, https://doi.org/10.1130/G33279.1, 2012.

Wittkop, C., Bartley, J. K., Krueger, R., Bouvier, A., Georg, R. B., Knaeble, A. R., St. Clair, K., Piper, C., and Breckenridge, A.: Influence of provenance and transport process on the geochemistry and radiogenic (Hf, Nd, and Sr) isotopic composition of Pleistocene glacial sediments, Minnesota, USA, Chemical Geology, 532, 119 390, https://doi.org/10.1016/j.chemgeo.2019.119390, 2020.

https://doi.org/10.5194/egusphere-2025-3920
Preprint. Discussion started: 19 September 2025
© Author(s) 2025. CC BY 4.0 License.

Young, J. M., Reyes, A. V., and Froese, D. G.: Assessing the ages of the Moorhead and Emerson phases of glacial Lake Agassiz and their temporal connection to the Younger Dryas cold reversal, Quaternary Science Reviews, 251, 106 714, https://doi.org/10.1016/j.quascirev.2020.106714, 2021.

Zhou, W., Wang, Q., Chen, S., Chen, F., Lv, H., Li, J., Chen, Q., Zhou, J., and Liang, B.: Nitrate leaching is the main driving factor of soil calcium and magnesium leaching loss in intensive plastic-shed vegetable production systems, Agricultural Water Management, 293, 108 708, https://doi.org/10.1016/j.agwat.2024.108708, 2024.